Proceedings of ASME Turbo Expo 2011
GT2011
June 6-10, 2011, Vancouver, British Columbia, Canada

GT2011-45100

CONDITIONAL MOMENT CLOSURE LES MODELLING OF AN AERO-ENGINE COMBUSTOR AT RELIGHT CONDITIONS

Simon R. Stow
Marco Zedda
Rolls-Royce plc
Derby, UK

Antonios Triantafyllidis
Andrew Garmory
Epaminondas Mastorakos
Cambridge University, UK

Thomas Mosbach
German Aerospace Center (DLR)
Stuttgart, Germany

ABSTRACT

A Conditional Moment Closure (CMC) approach embedded in an LES CFD framework is presented for simulation of the reactive flow field of an aero-engine combustor operating at altitude relight conditions. Before application to the combustor geometry, the CMC model was validated on the standard lab-scale Sandia flame D. For the combustor simulation, a global mechanism for *n*-heptane was used along with a Lagrangian approach for the spray, to which a secondary break-up model was applied. The simulation modelled a multi-sector sub-atmospheric rig that was used to verify the altitude relight capability of the combustor. A comprehensive suite of diagnostics was applied to the rig test, including high-speed OH and kerosene PLIF as well as high speed OH* chemiluminescence. The CMC-based CFD simulation was able to predict well the position of the flame front and fuel distribution at the low pressure, low temperature conditions typical of altitude relight. Furthermore, the simulation of the ignition showed strong similarities with OH* chemiluminescence measurements of the event. An EBU-based LES was run too and showed to be unable to capture the flame front as well as the CMC model could. This work demonstrates that CMC LES can be an effective tool to support assessment of the relight capability of aero-engine combustors.

NOMENCLATURE

CFD	Computational fluid dynamics
CMC	Conditional moment closure
DLR	Deutsches Zentrum fuer Luft- und Raumfahrt
EBU	Eddy break up
LES	Large eddy simulation
PDF	Probability density function
PRECISE	Predictive system for real engine combustors with improved sub-models and efficiency
RANS	Reynolds-averaged Navier–Stokes
RMS	Root mean square
RR	Rolls-Royce plc
RRD	Rolls-Royce Deutschland Ltd & Co KG
SMD	Sauter mean diameter

INTRODUCTION

Achievement of satisfactory relight capability is a key requirement in aero-engine design. The combustor relight capability is a function of the detailed aerodynamics of the combustion system as well as the overall combustion volume. Furthermore, it depends on the optimisation of the spark ignition parameters like spark position and effective energy introduced in the combustor. In general, increasing the combustor volume makes altitude relight easier, but introduces NOx penalties associated with increased combustor residence time as well as the requirement for cooling larger liner surface areas. The need to fix the combustor volume at an early stage of the design process to define the general layout of the component makes it particularly important to assess the corresponding implications on the relight capability. Over the years, aero-engine manufacturers have developed combustor design rules for relight. Application of these rules allows achieving the right ballpark relight capability. To date, verification of the actual altitude relight capability of combustors has been carried out mostly by means of sub-atmospheric testing, both in sector and full annular facilities. Detailed knowledge of the combustor relight capability for a range of pressure and mass-flow conditions is important also due to the uncertainty affecting the prediction of such parameters for a windmilling engine after a flame out at altitude.

Experimental research on ignition of spray flames is documented by a number of papers [1,2,3,4,5]. A review summarizing the fundamental issues associated with spark

ignition of non-premixed systems has become available [6], while a list of papers of lab-scale and combustor-scale spark ignition work is included in [7]. Detailed experimental investigation of the altitude relight process with advanced measurement techniques is still challenging due to several reasons. Firstly, the sub-atmospheric rig has to be provided with optical access for the laser diagnostics. While several optical and laser-based techniques have successfully been applied in gas turbine combustors, altitude relight conditions introduce unique challenges such as icing of the windows, dense sprays, liquid films on walls and optical windows. Recently, high speed imaging in the UV and visible range as well as laser induced fluorescence measurements have been performed at the altitude relight test rig of Rolls-Royce, Derby [8,9,10,11,12]. A Rolls-Royce Deutschland development injector was tested at 287 K and 0.5 bar. The measurements performed during this test have then been used to validate the CFD simulation of the reactive flow at altitude relight conditions and the ignition event that is presented in this paper.

Application of LES techniques to aero-engine combustors is becoming increasingly popular. The ability to resolve the larger, energy-containing scales directly, which is offered by LES methods, is particularly appealing for simulation of free shear flows. (For further information on combustion LES see [13] and references therein.) At the same time, development and application of Conditional Moment Closure (CMC) models has progressed significantly in the last few years; see for example [14] and references therein. The CMC is based on the fact that fluctuations of reactive scalars that are conditional on the mixture fraction are significantly smaller than fluctuation of the unconditional ones. This implies that closure of the chemical source term can be calculated as a function of mixture fraction conditional means. CMC models, which are particularly suitable for unsteady problems, have recently been embedded in an LES framework and used to simulate a number of lab-scale flames [14,15].

The present work is based on application of CMC LES to simulation of an industrial combustor at sub-atmospheric conditions. Rolls-Royce in-house combustion CFD code, PRECISE, was run in CMC LES mode and prediction compared against available measurements.

EXPERIMENTAL SET UP AND MEASUREMENT TECHNIQUES

The altitude relight test rig at the Rolls-Royce Strategic Research Centre (SRC) has been used to test relight performance of an aero combustor. The facility can operate down to inlet pressures of 0.2 bar, inlet temperature of 240 K and airflows up to 0.8 kg/s. The test section is provided with a quartz window. The test described here was performed on a configuration where one of the two sectors was fitted with an injector, the other one with a dummy, non-swirling device with the same effective area as the injector to be tested but no fuel injection. (The reason for not fuelling one of the sector was to give good visibility of the flame in the other sector. In particular, the air flow through the dummy injector, together with the air sheet along the side window, were necessary to prevent kerosene layers on the side window) The igniter used was a standard capacitor igniter, producing sparks at a frequency up to 2 Hz.

High-speed imaging of the OH* chemiluminescence and of the broadband flame luminescence at a repetition rate of 3500 Hz were applied to visualize both the transient flame initiation phenomena and the combustion behaviour of the steady burning flames. A LaVision HighSpeedStar 5 camera was used for the high-speed imaging of the broadband luminescence in the spectral range between 350 nm and 1000 nm. The exposure time was set to 1/15000 seconds. For the high-speed imaging of the OH* chemiluminescence in the ultraviolet spectral range around 310 nm, a lens-coupled two-stage high-speed image intensifier (LaVision HS IRO 25) was connected to the high-speed camera. The gate of the image intensifier was set to 100 µs. The flame luminosity was filtered by two high-reflecting mirrors and two combined interference filters. For the safety of the image intensifier, it was necessary to ensure the entire recording time was less than 500 ms to avoid imaging the following spark.

For the simultaneous OH and kerosene PLIF measurements, pulsed laser radiation in the ultraviolet spectral range was provided by a frequency-doubled Nd:YAG laser (Spectra-Physics PIV-400-10) pumping a tuneable dye laser (Sirah PRSC-G-24-EG) at 10 Hz repetition rate. The dye-laser was tuned to the Q1(8) transition at approximately 283 nm within the vibrational band v''=0, v'=1 of the OH $A^2\Sigma^+$-$X^2\Pi$ system. A small portion of the laser beam was deflected into a methane-air reference flame stabilized on a McKenna-type burner. The LIF signal produced by the flame was used for the online monitoring of the spectral position of the excitation line. Appropriate optics were used to expand the laser beam into a vertical sheet. The laser sheet inside the combustor was 65 mm in height and approximately 0.5 mm in thickness. The measurement plane of the PLIF experiments was parallel to the burner exit plane. The OH and the kerosene fluorescence generated within the laser excitation volume inside the combustion chamber were simultaneously imaged through the entrance window of the laser sheet by two camera systems (LaVision Imager Intense 3 with image intensifier IRO 25). The gates of the image intensifiers for the kerosene and OH fluorescence imaging were set to 300 ns and 500 ns respectively. The OH fluorescence was detected in the same narrow spectral range as the OH* chemiluminescence. The kerosene fluorescence was detected in the spectral range between 310 and 420 nm. More details of the experimental set-ups can be found in [10].

The section of the combustion chamber that is imaged by the cameras is shown by the photo in Fig. 1. The injector is located on the left side and the spark igniter can be seen in the top plate. The combustion chamber converges towards the exit at the right side.

Figure 1. Photograph of the combustion chamber. The injector is located on the left side; the spark igniter can be seen in the top plate.

THE CFD CODE

PRECISE is a RR in-house CFD code specifically developed for simulation of gas turbine combustors [16]. It is a parallel multi-block structured finite-volume code based on an implicit second-order accurate and bounded convection scheme [17], Cartesian velocities to avoid grid-aligned curvature terms and a co-located (non-staggered) approach for the velocity–pressure coupling [18]. It includes a number of RANS turbulence models, ranging from the standard k–epsilon model to Reynolds stress models, as well as LES capability, including the dynamic Smagorinsky sub-grid stress model. A host of turbulent combustion models for reacting scalars are available, including EBU, presumed PDF, transported PDF and flamelet generated manifold models, as well as several approaches to represent combustion chemistry, such as the two-step Westbrook and Dryer chemical kinetic model.

CMC MODEL

Because reaction rates are highly non-linear functions of species concentrations and temperature, we cannot take average reaction rates to be functions of average species and temperatures,

$$\overline{\dot{\omega}}_i \neq f(\overline{Y}_1, \overline{Y}_2, \ldots, \overline{Y}_n, \overline{T}) \tag{1}$$

However, the species and temperature are closely related to the instantaneous mixture fraction. CMC solves equations for the conditional averages, that is, the average value for a given mixture fraction. The conditional average, $\langle Y_i|\xi = \eta\rangle$, is a function of η (mixture-fraction space), plus space and time. The conventional average is related to the conditional average by

$$Y_i = \int_0^1 \langle Y_i | \eta \rangle P(\eta, x, t) \mathrm{d}\eta \tag{2}$$

where P is the mixture-fraction PDF, for example, a beta function, $\beta(\overline{\xi}, \overline{\xi'^2})$. The CMC equation for the conditional mass fraction of species i is

$$\frac{\partial \langle Y_i|\eta\rangle}{\partial t} + \langle u|\eta\rangle \cdot \nabla \langle Y_i|\eta\rangle - \langle N|\eta\rangle \frac{\partial^2 \langle Y_i|\eta\rangle}{\partial \eta^2} = \langle \dot{\omega}_i|\eta\rangle + \frac{1}{\rho P(\eta)} \nabla \cdot \left(\rho P(\eta) D_t \nabla \langle Y_i|\eta\rangle\right) \tag{3}$$

where $N = D\nabla\xi\cdot\nabla\xi$, is the scalar dissipation. There is a similar equation for the conditional temperature, $\langle T|\eta\rangle$. For first-order CMC, one assumes that the conditional reaction rates are functions of conditional species and temperatures,

$$\langle \dot{\omega}_i | \eta \rangle = f(\langle Y_1 | \eta \rangle, \langle Y_2 | \eta \rangle, \ldots, \langle Y_n | \eta \rangle, \langle T | \eta \rangle) \tag{4}$$

Implementation of the CMC model in LES is relatively recent, with only a few papers available (see [14,15,19] and references therein). There are a large number of sub-models that need to be prescribed concerning the conditional velocity, $\langle u|\eta\rangle$, the conditional scalar dissipation, $\langle N|\eta\rangle$, and the sub-grid diffusivity, D_t, and some choices concerning the correspondence between the LES and the CMC grids (see later) have to be made. For details, the reader must consult [14,15,19].

VALIDATION BASED ON LAB-SCALE FLAME

As part of this work, the implementation of the CMC model in PRECISE has been tested by simulating the Sandia flame D, a piloted methane–air flame for which extensive temperature, velocity and species measurements are available. This is part of a greater effort to predict extinction with LES-CMC that has resulted in very good predictions of the very challenging flame F [15]. There is a central circular jet of diameter 7.2 mm, which is composed of a rich mixture of methane and air. This is surrounded by annular pilot of hot products. Simulations used a structured multi-block mesh of 65 blocks and about 1.3 million cells. A 19-species reaction mechanism for methane was used on a CMC grid of 23×23×23 = 12167 cells, with 51 points in mixture-fraction space. Both the CFD and CMC grids were concentrated on the inlet, becoming coarser further away from the jet. Figures 2 and 3 show instantaneous results for temperature and CO concentration. In Figs. 4 and 5, mean and RMS values are compared with measurements in the plane 7.5 jet-diameters downstream of the inlet, while conditional values compared in Figs. 6 and 7. A similar level of agreement was found for other planes at various distances from the burner. (Further details on the flame D calculation, as well as calculations for flame F, can be found in [15].)

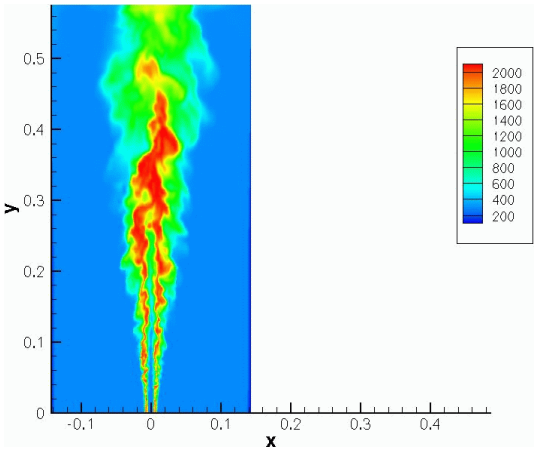

Figure 2. Instantaneous temperature through the jet centre for CMC LES calculation of Sandia flame D.

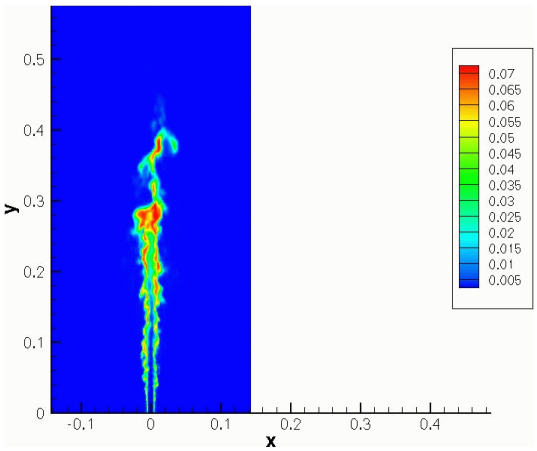

Figure 3. Instantaneous CO concentration through the jet centre for CMC LES calculation of Sandia flame D.

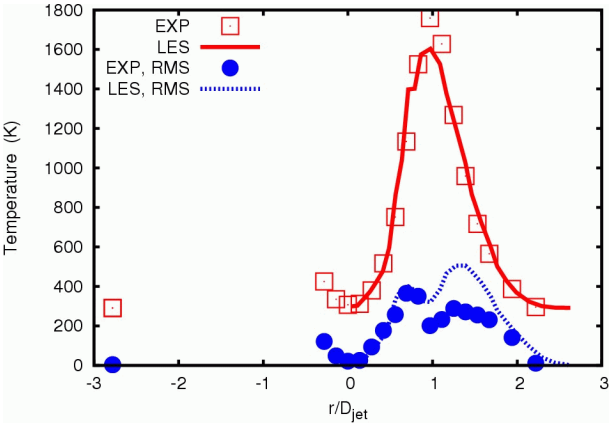

Figure 4. Comparison of measurements and CMC LES predictions for mean and RMS of temperature as a function of radius at y = 0.054 m for Sandia flame D.

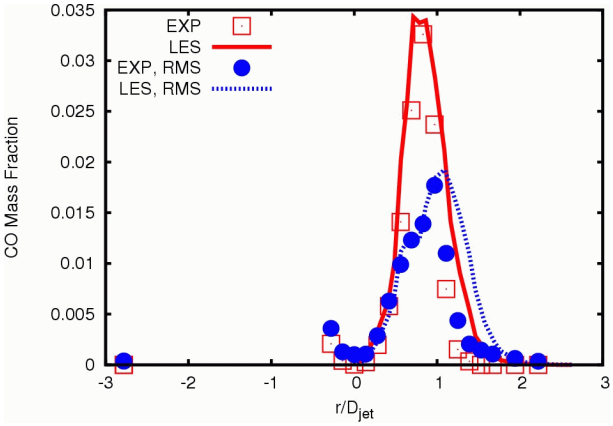

Figure 5. Comparison of measurements and CMC LES predictions for mean and RMS of CO concentration as a function of radius at y = 0.054 m for Sandia flame D.

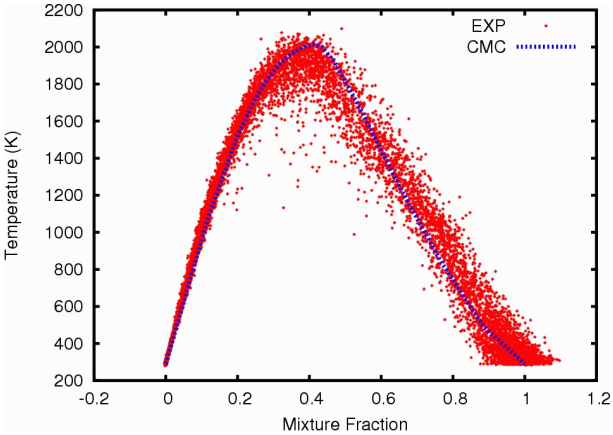

Figure 6. Comparison of measurements and CMC LES predictions for conditional temperature using data in the plane y = 0.054 m for Sandia flame D.

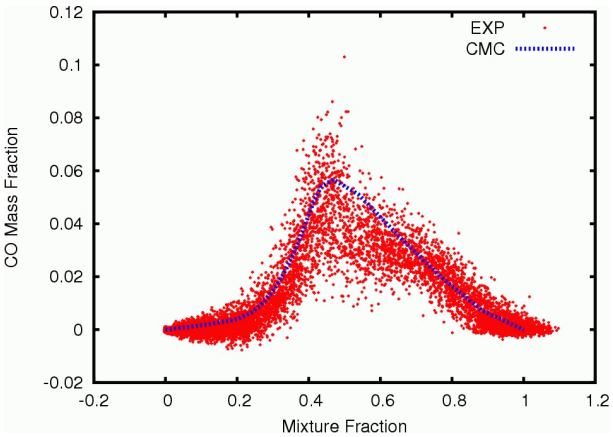

Figure 7. Comparison of measurements and CMC LES predictions for conditional CO concentration using data in the plane y = 0.054 m for Sandia flame D.

It can be concluded that the present LES-CMC implementation with the code PRECISE gives very good results for simple flames. For recirculating methane igniting flames [15], the results were also very good concerning the overall flame expansion, while the PRECISE code has also resulted in very good agreement with experimental data for unsteady bluff-body flows [20].

REACTION MECHANISM USED FOR SIMULATION OF KEROSENE AT ALTITUDE RELIGHT CONDITIONS

In the current modelling study of spray flame ignition and propagation the principal quantity needed from the chemical reaction model is the heat release rate. To this end the simple one step reaction model proposed by Richardson for *n*-heptane [21,22], based on the fitting methodology of Fernandez-Tarrazo et al. [23] has been used. The model expresses the heat of reaction and the Arrhenius activation temperature as functions of equivalence ratio. This achieves the correct laminar premixed flame speed for methane-air flames and realistic diffusion flame structures even close to extinction [21]. The *n*-heptane oxidation model is given by,

$$C_7H_{16} + 11O_2 \rightarrow 7CO_2 + 8H_2O + q \tag{5}$$

with a global reaction rate (mol.cm^{-3}s^{-1}) of the form,

$$\omega = Be^{-T_a/T} \Gamma_{C_7H_{16}} \Gamma_{O_2} \tag{6}$$

and the heat release due to complete oxidation of one mole of fuel given by,

$$q_0 = h_{C_7H_{16}} - 7h_{CO_2} - 8h_{H_2O} = 5401\ \text{kJ.mol}^{-1} \tag{7}$$

The reduced heat release resulting from incomplete combustion at rich equivalence ratios is modelled by,

$$\begin{cases} \phi \le 1 : q/q_0 = 1 \\ \phi > 1 : q/q_0 = 1 - \alpha(\phi - 1) \end{cases} \tag{8}$$

The parameters selected in order to model partially premixed *n*-heptane combustion at atmospheric conditions were $\alpha = 0.18$, $T_{a0} = 15000$ K and $B = 2.4\text{x}10^{14}$ cm^3.mol^{-1}s^{-1} as discussed in [21]. T_a was expressed as,

$$\begin{cases} \phi \le 0.74 : T_a/T_{a0} = 1 + 1.6948(\phi - 0.74)^2 \\ 1.13 \ge \phi > 0.74 : T_a/T_{a0} = 1 \\ \phi > 1.13 : T_a/T_{a0} = 1 + 0.0092(\phi - 1) + 0.9423(\phi - 1.13)^2 \end{cases} \tag{9}$$

This fit produces the variation of premixed laminar flame speed with equivalence ratio shown in Fig. 8.

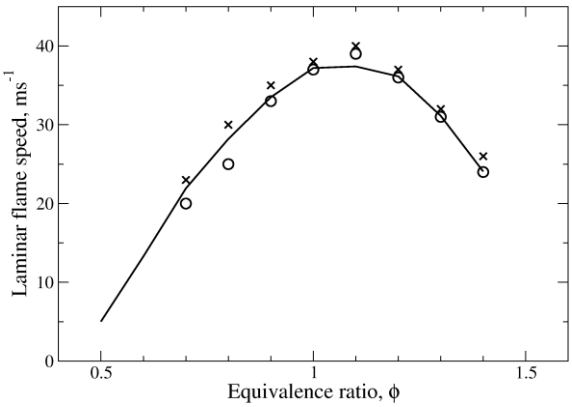

Figure 8. The modelled flame *n*-heptane laminar flame speed versus equivalence ratio at 1 bar and 300 K, compared to experimental measurements. From [21].

Note that the use of *n*-heptane of atmospheric conditions instead of kerosene at relight conditions induces an uncertainty for the flame speed of the fuel in the real device. However, recent simulations of laminar flames with detailed mechanisms for *n*-heptane and decane, which is a close surrogate to kerosene as far as flame speed is concerned, showed that, (1) the two fuels have flame speeds within 10%, and (2) the low-temperature, low-pressure conditions did not change the flame speed appreciably [24]. Therefore the data shown in Fig. 8 could be used realistically for the altitude relight simulations, in the absence of a better validated mechanism.

SPRAY MODEL USED IN THE ALTITUDE RELIGHT SIMULATION

Considering the importance of fuel placement for altitude relight, a summary of the spray model used is here provided. In PRECISE, an Eulerian–Lagrangian approach is used to couple the gas and liquid phase, with the particle trajectories of spray droplets being tracked. Rather than track individual droplets, a parcel approach is used. A parcel (or "size classes") represents a number of droplets assumed to have the same conditions, in particular the same diameter. The number of droplets need not in fact be an integer (it is the number flow rate, rather than the number of droplets, that is the important quantity).

A primary break-up model can be used to simulate the initial film break-up process, or alternatively droplets can be introduced at some location downstream of this process with a specified SMD. The droplet diameters are typically assumed to follow the modified Rossin–Rammler distribution of Custer and Rizk [25]. In steady calculations, the distribution is represented by a discrete set of parcel diameters, and complete path of each parcel through the domain is calculated. In unsteady calculations, at each time step the current locations of the parcels are updated according to their trajectories, and new parcels are introduced with diameters randomly chosen from the distribution. In either case, the initial number flow rate of the parcel is determined by the fuel flow rate.

The secondary break-up model in PRECISE is composed of two sub-models: a disintegration mechanism and a stripping mechanism. The stripping mechanism gives a continuous reduction in the droplet diameter if the Weber number exceeds a critical value. If the Weber number is above the critical value for longer than a critical time period, the disintegration mechanism gives a discrete diameter change. Each droplet is assumed to break-up into two droplets of equal size, hence the parcel diameter is reduced by a factor of $2^{1/3}$. Note that in both mechanisms, there is no creation of new parcels or exchange with other parcels. The mass of the parcel is conserved, and hence any reduction in diameter is accompanied with an increase in number flow rate.

Evaporation of the droplets is based on the single-component infinite-conductivity model (see [26,27]). The rate of evaporation depends on droplet's diameter and conditions, the local gas conditions, and the relative velocity between the gas and the droplet. The droplet diameter reduces according to the mass evaporated, while for the gas, this becomes a source of mass (with corresponding sources for momentum, energy, and mixture fraction).

There is a choice of three different wall boundary conditions for spray: droplets are either assumed to evaporate instantly on hitting a wall, reflect off the wall, and slide along it.

Further details on the spray modelling in PRECISE (including the primary break-up model) are given in [28].

SIMULATION OF ISOTHERMAL CONDITIONS

The operating conditions chosen for modelling in the CFD calculations are given in Table 1.

Air pressure	55.2 kPa
Air temperature	278 K
Fuel temperature	288 K

Table 1. Operating conditions modelled in CFD simulations.

An initial isothermal simulation of a single sector of the rig was done, which included modelling of the flows through the injector. The hexa-dominant unstructured mesh, shown in Figs. 9 and 10, had roughly 5 million cells. An unstructured version of the PRECISE code was used for this calculation.

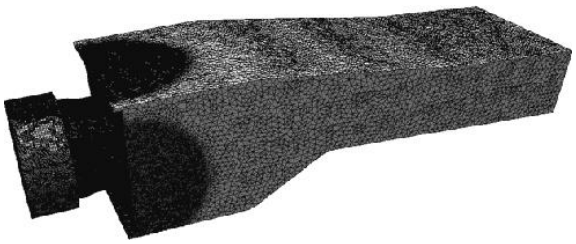

Figure 9. Overview of mesh for the "through-the-swirler" model.

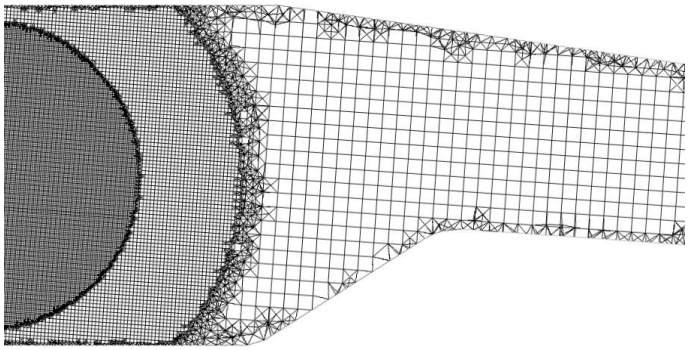

Figure 10. Section of unstructured mesh in injector centreline plane for initial "through-the-swirler" model.

The results were used to derive boundary conditions for the subsequent calculations, which started from the trailing edge of the swirler vanes. Both sectors were included in the model (see Fig. 11) and a structured multi-block mesh of 169 blocks and about 8 million cells was used (see Fig. 12).

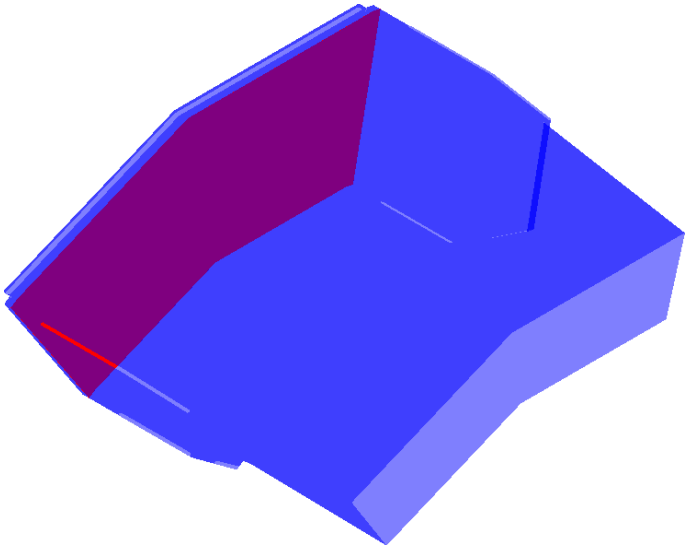

Figure 11. Extent of the computational domain for the CMC LES.

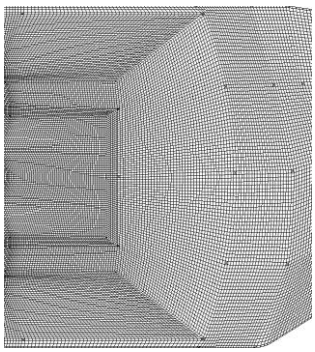

Figure 12. Details of the multi-block structured grid.

Steady RANS calculations used the standard k–ε model, while LES calculations used the dynamic Smagorinsky model. Fuel was introduced at a ring of points slightly downstream of the injection point. No primary spray break-up model was used, and instead the initial SMD was taken to be 80 μm. Calculations used the PRECISE secondary break-up model. A CMC grid of 24×24×23 = 13248 cells (see Fig. 13) was used. This was concentrated close to the injector in order to capture the high variation in strain rate expected here. (Away from the injector, any combustion is expected to be a low strain rates. There will be little variation in the flamelet and so the CMC grid can very coarse.) 51 points in mixture-fraction space were used.

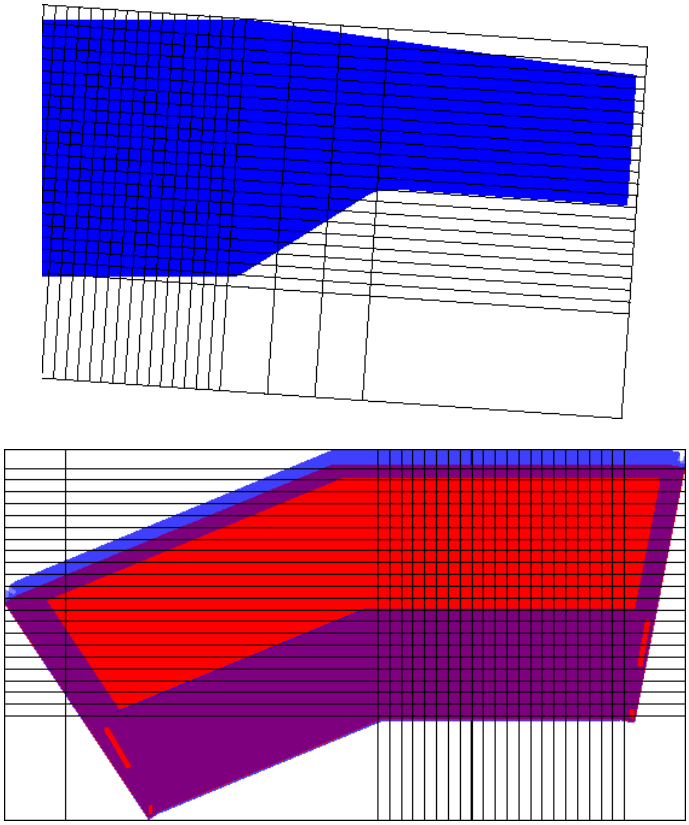

Figure 13. CMC mesh used.

To begin with, non-reacting calculations on the two-sector model were performed. Figure 14 shows the normalized velocity-magnitude results for a steady k–ε calculation. This solution was then used to initialise a LES calculation. The time step used was 5 μs (resulting in a maximum Courant number of 0.91). Instantaneous and time-average results for velocity magnitude are shown in Figs. 15 and 16. The time average (calculated over 10 ms) is seen to be quite similar to the k–ε solution.

The spray wall boundary condition used in both the k–ε and LES was to assume that droplets reflect off walls. Although this is recognized to be a crude assumption, it was deemed that the resulting inaccuracy would be comparable with the one associated with the primary break up.

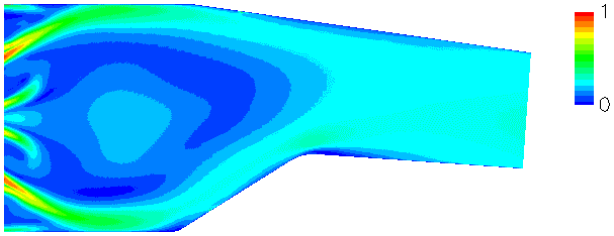

Figure 14. Normalized velocity magnitude contour on injector centreline plane from non-reactive k–ε.

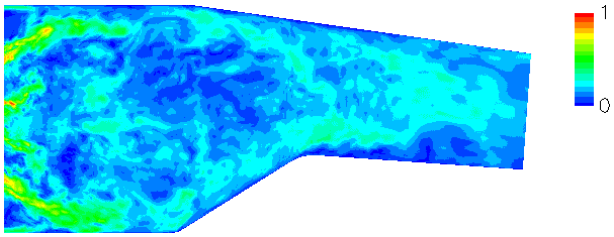

Figure 15. Instantaneous normalized velocity magnitude contour in injector centreline plane for non-reacting LES.

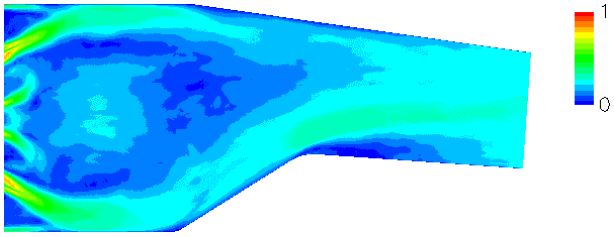

Figure 16. Time-averaged normalized velocity magnitude contour in injector centreline plane for non-reacting LES.

VALIDATION OF REACTIVE MODELS AT ALTITUDE RELIGHT CONDITIONS

The non-reacting k–ε solution was used to initialise a steady combusting EBU calculation (using the two-step Westbrook and Dryer chemical kinetic model), which was run to obtain a first result using limited computational resources. Some results are shown in Figs. 17–21.

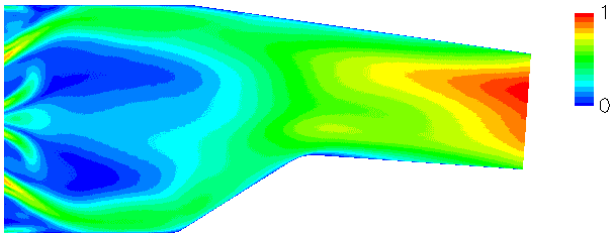

Figure 17. Normalized velocity magnitude in injector centreline plane for EBU k–ε.

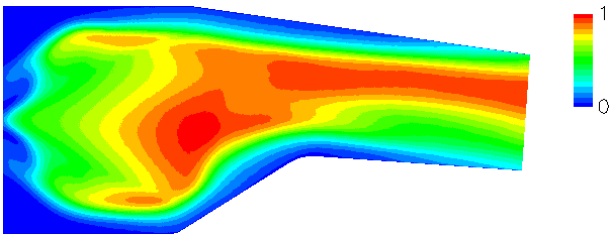

Figure 18. Normalized temperature in injector centreline plane for EBU *k*–*ε*.

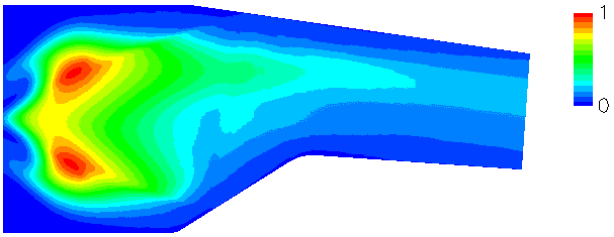

Figure 19. Normalized mixture fraction in injector centreline plane for EBU *k*–*ε*.

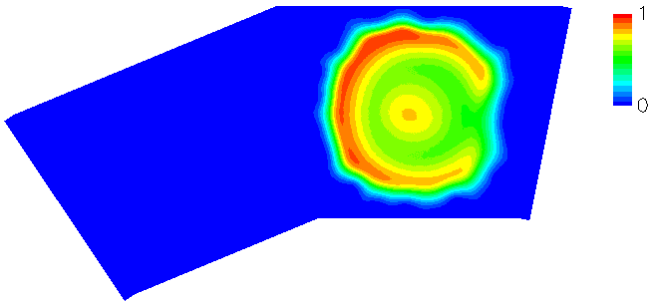

Figure 20. Normalized temperature in axial plane 35 mm downstream of injector face for EBU *k*–*ε*.

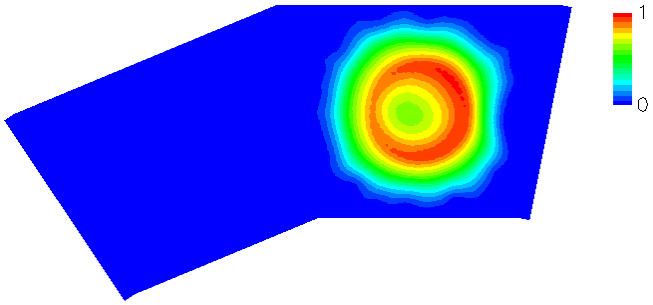

Figure 21. Normalized unburnt fuel concentration in axial plane 35 mm downstream of injector face for EBU *k*–*ε*.

Figures 22 and 23 show time-averaged broadband flame luminescence and OH* chemiluminescence images from the high-speed camera measurements performed on the SRC rig. The chemiluminescence images were subjected to Abel inversion on the assumption of axisymmetry of the flame. (Note that the flame is not perfectly axisymmetric, due to the asymmetry in cross-stream direction, but is approximately so.) The two OH* chemiluminescence distributions in the axial plane of the combustor shown in Fig. 23 correspond to two operating conditions bracketing the conditions for which the CFD was run. Figures 24 and 25 show ensemble-averaged filtered PLIF images of kerosene and OH density distributions. Filtering means that all images used for the ensemble-averaged image were post-processed in order to remove the scattered signal contributions from the fuel droplets. The corresponding time-resolved images were taken simultaneously.

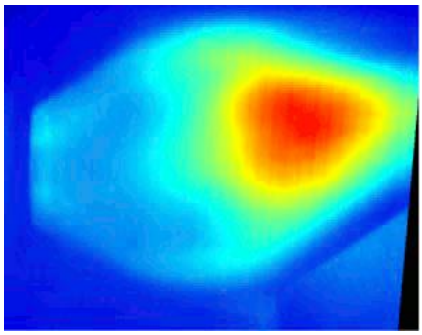

Figure 22. Measured time-averaged flame luminosity.

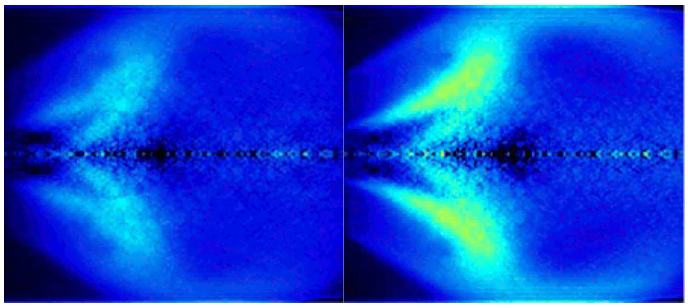

(a) (b)

Figure 23. Abel-inversed images of the time-averaged OH* chemiluminescence distributions, for two operating conditions bracketing the conditions used in the CFD. The field of view is 104.5 mm × 92.1 mm.

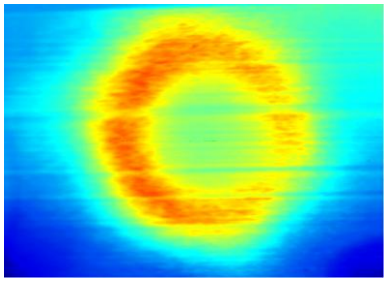

Figure 24. Measured ensemble-averaged filtered PLIF images of kerosene density distribution. The field of view is 67 mm x 48 mm.

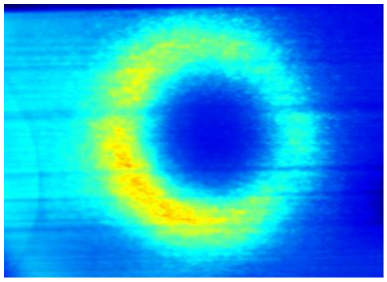

Figure 25. Measured ensemble-averaged filtered PLIF images of OH density distribution. The field of view is 67 mm x 48 mm.

The injector flow field predicted by the k–ε reactive simulation is quite similar to the non-reacting case. The large temperatures towards the back of the combustor are consistent with the large flame luminosity seen in this region in the experiments (comparing Figs. 18 and 22). However, the flame structure close to the injector (Fig. 23) is not captured. The unburnt fuel concentration (Fig. 21) is quite similar in the kerosene PLIF measurements (Fig. 24).

Steady k–ε calculations were also performed using equilibrium presumed PDF, as well as using 0D-CMC with the one-step *n*-heptane mechanism. "0D-CMC" refers to a calculation for which the spatial variation in the CMC equations is ignored. In practice, a fixed value of maximum scalar dissipation rate is chosen and the CMC conditional variables are found from a separate initial calculation. For the one-step *n*-heptane mechanism a fixed maximum scalar dissipation rate of 50 s^{-1} was used. (This value is fairly arbitrary; the aim is simply to have a "typical" burning flamelet.). The CMC conditional variables are then used in the CFD calculation, which essentially become equivalent to a presumed PDF approach, however the resulting solution is a useful starting point for a true "3D" CMC calculation. Results for the presumed PDF and 0D-CMC calculations (not shown here) were all fairly similar, however good convergence was not achieved for these cases (probably due to inherent unsteadiness in the flow). Large temperatures at the back of the combustor and the unburnt fuel concentration in the PLIF measurement plane were similar to in the EBU calculation. Unlike the EBU results, there was some suggestion of the flame structure close to the injector, although too far upstream.

A CMC LES calculation was performed with the one-step *n*-heptane mechanism, initialised from the corresponding 0D-CMC k–ε. As in the non-reacting LES calculations, a time step of 5 μs was used (resulting in a maximum Courant number of 0.85 in this case). Instantaneous and time-average results are shown in Figs. 26–33 (with time averages calculated over 5 ms). Some evidence of the CMC grid can be seen in the temperature close to the injector, suggesting that the CMC grid is not fine enough here. Despite this, the shape and location of the flame front close to the injector appear to be quite well captured (Fig. 29).

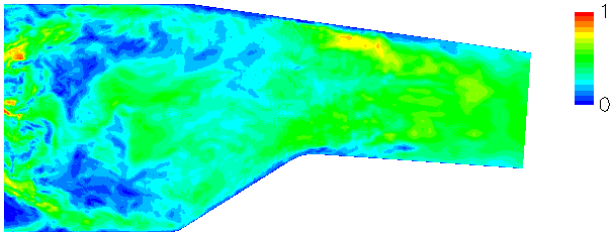

Figure 26. Instantaneous normalized velocity magnitude in injector centreline plane for CMC LES.

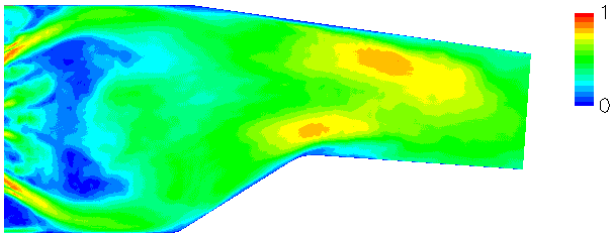

Figure 27. Time-average normalized velocity magnitude in injector centreline plane for CMC LES.

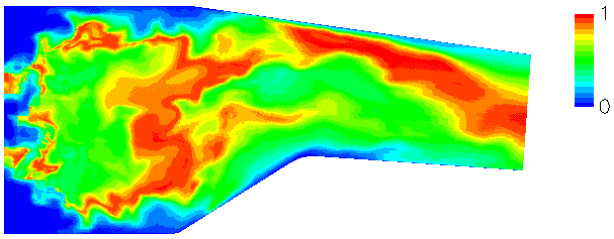

Figure 28. Instantaneous normalized temperature in injector centreline plane for CMC LES.

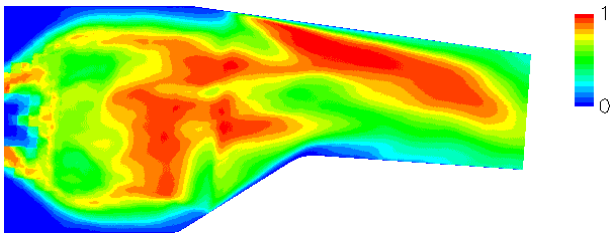

Figure 29. Time-averaged normalized temperature in injector centreline plane for CMC LES.

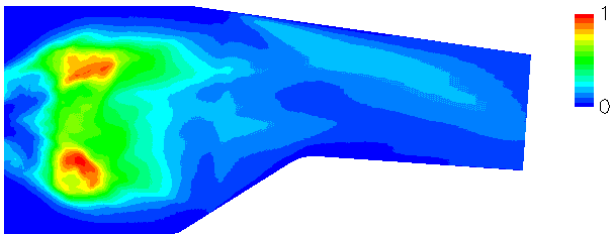

Figure 30. Time-averaged normalized mixture fraction in injector centreline plane for CMC LES.

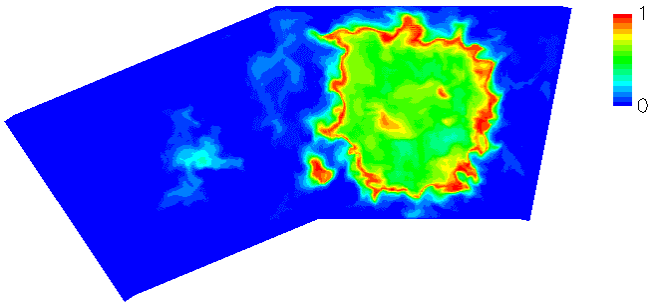

Figure 31. Instantaneous normalized temperature in axial plane 35 mm downstream of injector face for CMC LES.

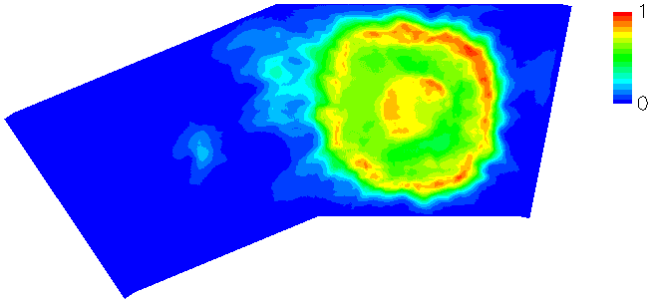

Figure 32. Time-averaged normalized temperature in axial plane 35 mm downstream of injector face for CMC LES.

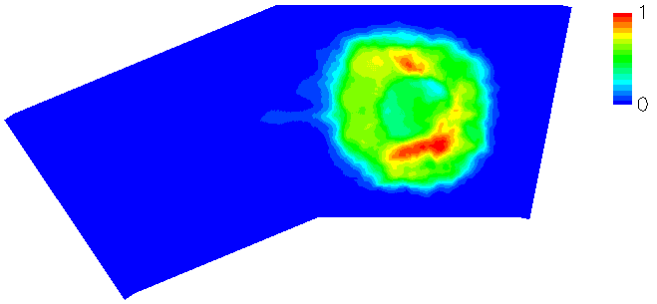

Figure 33. Time-averaged normalized unburnt fuel concentration in axial plane 35 mm downstream of injector face for CMC LES.

Results from an EBU LES calculation are given in Figs. 34–37. The results look very different to the EBU k–ε case. The flame structure close to the injector is fairly similar to the CMC LES results, however there are very large temperatures close to the injector, which seems inconsistent with the flame luminosity measurements (see Fig. 22).

For the CMC LES, the computation time per iteration was found to be about twice that of the non-reacting LES simulation. By comparison, the EBU LES calculation was around 20% slower than non-reacting LES.

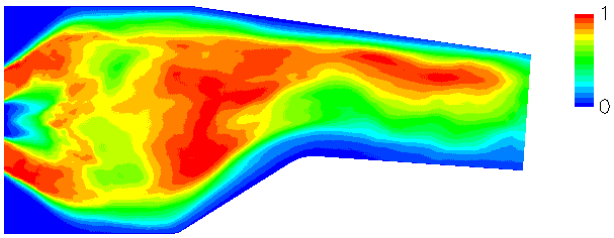

Figure 34. Time-averaged normalized temperature in injector centreline plane for EBU LES.

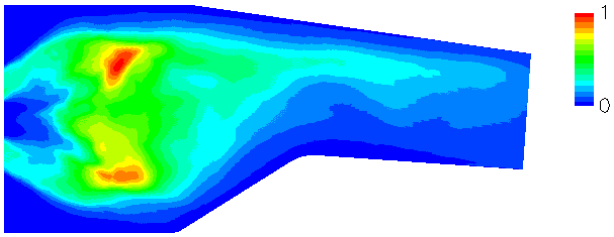

Figure 35. Time-averaged normalized mixture fraction in injector centreline plane for EBU LES.

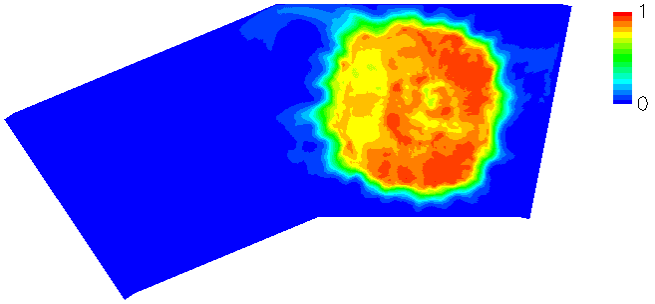

Figure 36. Time-averaged normalized temperature in axial plane 35 mm downstream of injector face for EBU LES.

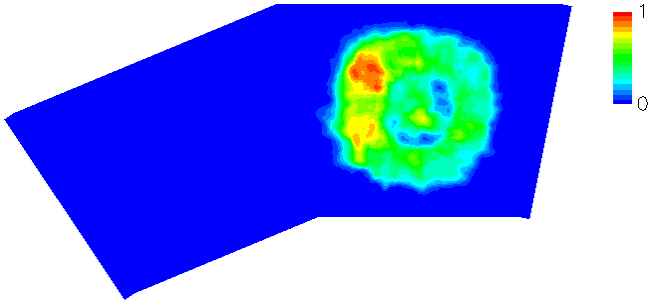

Figure 37. Time-averaged normalized unburnt fuel concentration in axial plane 35 mm downstream of injector face for EBU LES.

VALIDATION OF CMC LES OF IGNITION EVENT

Simulation of the spark ignition process was attempted as well. A CMC LES calculation was initialised from an inert-CMC LES solution. This inert solution was effectively equivalent to a non-reacting LES, however the spray wall boundary condition was changed to be complete evaporation at the walls. Figure 38 shows mixture-fraction results for the solution.

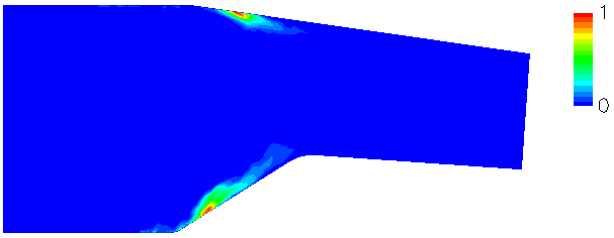

Figure 38. Instantaneous normalized mixture fraction in injector centreline plane for inert-CMC LES with spray evaporation at walls.

Large values can be seen at locations on the inner and outer walls where the spray cone impinges. About 60% of the fuel evaporated in this case. Without this change to the spray wall boundary condition, very little evaporation occurred and mixture-fraction values were extremely low (being less than 3×10^{-3} throughout the domain), and as a result, high temperatures were never attained when spark ignition simulations were attempted.

In the ignition simulation, the spark-induced plasma was modelled by initialising the CMC conditional variables in some cells to be a burning flamelet solution, instead of the inert conditions used elsewhere. (The burning flamelet used was a 0D-CMC solution). A region of 5×5×5 CMC cells located around the ignitor in the outer wall was chosen for the "spark", as shown in Fig. 39.

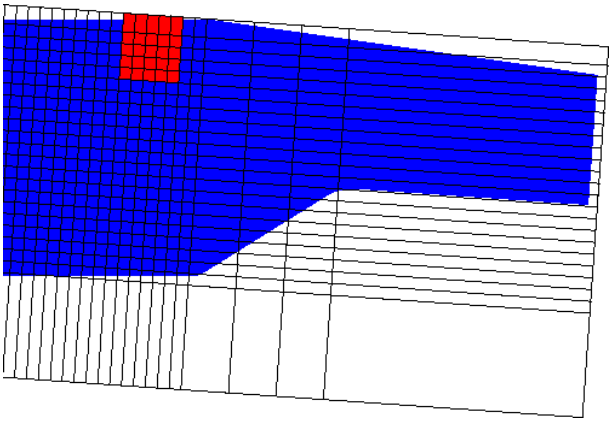

Figure 39. CMC grid used for ignition simulation in injector centreline plane, with "spark" CMC cells.

The size of this region was chosen to be comparable to that seen in the first image of Fig. A1, which shows the measured time series of OH* chemiluminescence during ignition, for operating conditions comparable to those modelled in LES. (Although the measurements in the first image appear saturated, it is clear that the red region is very hot, and the blue and black regions are cold, thus defining the approximate size and location of the spark-induced plasma.) The CMC equations were then solved in the usual way, however a relaxation coefficient of 0.5 was applied to the CMC solution to mitigate the impact of discontinuities created by introducing the spark plasma onto the convergence behaviour. The wall-evaporation boundary condition was maintained in the ignition simulation. Figure A2 shows a series of snapshots from the calculation. Although the burning-flamelet spark-plasma region protrudes significantly into the combustor, the initial temperature rise is only seen close to the wall, since away from the wall the mixture fraction is negligible. As the calculation progresses, the flame expands downwards (see 0–10 ms in the figure), and then upstream along the central recirculation zone (12–16 ms), (as well as being carried downstream), before attaching to the injector (see 21 ms). By 28 ms, the flame has fully established and appears very similar to the lit simulation discussed in the previous section. At 11 ms, a hot region appears on the inner wall. This is likely due to hot gases being carried from the outer wall to the inner wall by the swirling flow (outside of the injector centreline plane shown). Large discontinuities can sometimes be seen at the edges of some CMC cells at back of the flametube (see for example the snapshot at 14 ms, where the temperatures is cold close to the inner wall of the exit, but suddenly becomes hot above this). Clearly the CMC cells are too large in this region, however the impact on the ignition process in the front half does not seem to be great.

Similarity can be seen between these results and the OH* chemiluminescence measurements in Fig. A1 (note however that these are for slightly different operating conditions). In the measurements, the flame appears to expand downwards, then upstream, over very similar time scales to the simulation, and has expanded fully across the combustor after 20–30 ms. One difference seems to be that the downwards expansion in the measurements extends as far as the inner wall, which is not seen in Fig. A2. However, this could be because Fig. A2 shows results in a cut plane, while the measurements in Fig. A1 are "line of sight".

The assumption of complete evaporation of spray at the walls is clearly not realistic and an area for future improvements. The effect is to produced a highly ignitable fuel-air mixture close to the ignitor, meaning that the generation of the initial flame kernel is somewhat artificial. (Note however that in practise the spark plasma itself would induce evaporation). The fuel evaporated at the walls is convected downstream, not recirculated (see Fig. 38), and hence the subsequent propagation of the flame, which is of primary interest here, should still be representative.

SUMMARY AND CONCLUSIONS

CFD simulations have been performed of the altitude relight experiment of DLR-VT. The comprehensive suite of measurements taken on the Rolls-Royce rig test, including high-speed OH and kerosene PLIF as well as high speed OH* chemiluminescence, demonstrated that availability of such advanced diagnostics can provide very valuable insight into the flame generated by complex geometries for industrial applications.

CFD simulations have been performed of the altitude relight experiment of DLR-VT, using both steady k–ε and LES and two different combustion models. LES gave better results than corresponding k–ε RANS calculations. This confirmed the superiority of the LES approach for simulation of combustor flows. CMC LES (with one-step *n*-heptane mechanism) gave the best agreement with measurements. All combusting cases captured the hot region at the back of the combustor seen in flame luminosity measurements. EBU k–ε did not capture the flame structure close to the injector seen in OH* chemiluminescence measurements. Both CMC LES and EBU LES captured the location and shape of the detached flame quite well. However, the latter gave too high temperatures close to the injector. (Note that although the calculations were performed at sub-atmospheric altitude-relight conditions, the CMC approach here can be directly applied to high pressure / high power conditions, provided a suitable reaction mechanism is used.)

A spark ignition simulation using CMC LES successfully lit the combustor and showed similarity to measurements of the ignition process. In order to get ignition, it was necessary to assume evaporation of fuel at the walls.

A number of conclusions could be drawn. Firstly, as expected, the most significant uncertainty affecting the CFD simulations was due to the spray boundary conditions, imposed downstream of the primary break up, as well as the droplet wall interaction. Secondly, utilization of CMC LES in combination with a simple, one-step, calibrated reaction mechanism was enough to produce a quite accurate prediction of the flow field at altitude relight conditions. Lastly, a relatively coarse CMC grid was capable of providing a solution that matched measurements qualitatively well.

The work presented demonstrated how the proposed CFD approach can be directly used to support the combustor design for relight.

ACKNOWLEDGMENTS

The financial support of the TIMECOP-AE FP7 is gratefully acknowledged. The authors would like to thank Dr. Edward Richardson (University of Southampton) for providing support for the reaction mechanism. The support of Mr. Sermed Sadig (Rolls-Royce Deutschland) and Mr. Emmanuel Aurifeille (Rolls-Royce plc) in setting up of the CFD models is also acknowledged.

REFERENCES

[1] D. W. Naegeli and L. G. Dodge, 1991, “Ignition study in a gas turbine combustor”, Combustion Science and Technology, Vol. 80, pp. 165–184.

[2] S. K. Aggarwal, 1998, “A review of spray ignition phenomena: Present status and future research”, Progress in Energy and Combustion Sci, Vol. 24, pp. 565–600.

[3] G.. Pucher, G.. Wang, M. F. Bardon, D. P. Gardiner, A. M. Namet-Allah, and A. Benaissa, 2001, “Enhanced ignition systems for aircraft altitude relight”, 48th Annual Conference of the Canadian Aeronautics and Space Institute.

[4] A. Dreizler and J. Janicka, 2002, “Diagnostic challenges for gas turbine combustor model validation”, in K. Kohse-Hoinghaus and J. Jeffries (eds.), “Applied Combustion Diagnostics”, Taylor & Francis.

[5] G. Pucher and W. D. Allan, 2004, “Turbine fuel ignition and combustion facility for extremely low temperature conditions”, ASME paper GT2004-53620.

[6] E. Mastorakos, 2009, “Ignition of turbulent non-premixed flames”, Progress in Energy and Combustion Science, Vol. 35, pp. 57–97.

[7] T. Marchione, S. F. Ahmed, and E. Mastorakos, 2009, “Ignition of turbulent swirling n-heptane spray flames using single and multiple sparks”, Combustion and Flame, Vol. 156, pp. 166–180.

[8] R. W. Read, 2008, “Experimental investigations into high-altitude relight of a gas turbine”, Ph.D. thesis, University of Cambridge.

[9] R. W. Read, J. W. Rogerson, and S. Hochgreb, 2008, “Relight imaging at low temperature, low pressure conditions”, AIAA Paper 2008-0957.

[10] T. Mosbach, R. Sadanandan, W. Meier, and R. Eggels, 2010, “Experimental analysis of altitude relight under realistic conditions using laser and high-speed video techniques”, ASME Paper GT2010-22625.

[11] D. Fyffe, J. Moran, K. Kannaiyan, R. Sadr, and A. Al-Sharshani, 2011, “Effect of GTL-like jet fuel composition on GT engine altitude ignition performance – Part I: Combustor operability“, ASME Paper GT2011-45487.

[12] T. Mosbach, G. C. Gebel, P. Le Clerq, R. Sadr, K. Kannaiyan, and A. Al-Sharshani, 2011, “Investigation of GTL-like jet fuel composition on GT engine altitude ignition and combustion performance – Part II: Detailed diagnostics”, ASME Paper GT2011-45510.

[13] S. James, J. Zhu, and M. S. Anand, 2006, “Large-eddy simulations as a design tool for gas turbine combustion systems”, AIAA J., Vol. 44, No. 4, pp. 674–686.

[14] A. Triantafyllidis, E. Mastorakos, and R. L. G. M. Eggels, 2009 “Large eddy simulations of forced ignition of a non-premixed bluff-body methane flame

with conditional moment closure", Combustion and Flame, Vol. 156, pp. 2328–2345.

[15] A. Garmory and E. Mastorakos, 2011, "Capturing localised extinction in Sandia Flame F with LES-CMC", Proceedings of the Combustion Institute, Vol. 33, pp. 1673–1680.

[16] M. S. Anand, J. Zhu, C. Connor, and M. Razdan, 1999, "Combustor flow analysis using an advanced finite-volume design system", ASME Paper 99-GT-273.

[17] J. Zhu, 1992, "On the higher-order bounded discretization schemes for finite-volume computations of incompressible flows", Computer Methods in Applied Mechanics and Engineering, Vol. 98, No. 3, pp. 345–360.

[18] C. M. Rhie and W. L. Chow, 1983, "Numerical study of the turbulent flow past an airfoil with trailing edge separation", AIAA J., Vol. 21, No. 11, pp. 1525–1532.

[19] I. Stankovic, A. Triantafyllidis, E. Mastorakos, C. Lacor, and B. Merci, 2010, "Simulation of hydrogen auto-ignition in a turbulent co-flow of heated air with LES and CMC approach", to appear in Flow, Turbulence and Combustion.

[20] S. Ayache, J. R. Dawson, A. Triantafyllidis, R. Balachandran, and E. Mastorakos, 2010, "Experiments and large-eddy simulations of acoustically-forced bluff-body flows", International Journal of Heat and Fluid Flow, Vol. 31, pp. 754–766

[21] E. S. Richardson, 2007, Ph.D. thesis, University of Cambridge.

[22] E. S. Richardson and E. Mastorakos, 2007, "Conditional moment closure modelling for spark ignition in a turbulent n-heptane spray", 5th Mediterranean Combustion Symposium.

[23] E. Fernandez-Tarrazo, A. L. Sanchez, A. Linan, and F. A. Williams, (2006), "A simple one-step chemistry model for partially premixed hydrocarbon combustion", Combustion and Flame, Vol. 147, pp. 32–38.

[24] A. Neophytou and E. Mastorakos, 2009, "Simulations of laminar flame propagation in droplet mists", Combustion and Flame, Vol. 156, pp. 1627–1640.

[25] J. R. Custer and N. K. Risk, 1985, "Effect of fuel nozzle concept on spray quality and droplet size distribution", AIAA Paper 85-1186.

[26] J. S. Chin and A. H. Lefebvre, 1983, "Steady-state evaporation characteristics of hydrocarbon fuel drops", AIAA J., Vol. 21, No. 10, pp. 1437–1443.

[27] N. K. Risk and J. S. Chin, 1994, "Comprehensive fuel nozzle model", AIAA Paper 94-3278.

[28] C. M. Cha, J. Zhu, N. K. Risk, and M. S. Anand, 2005, "A comprehensive liquid fuel injection model for CFD simulations of gas turbine combustors", AIAA Paper 2005-0349.

ANNEX A

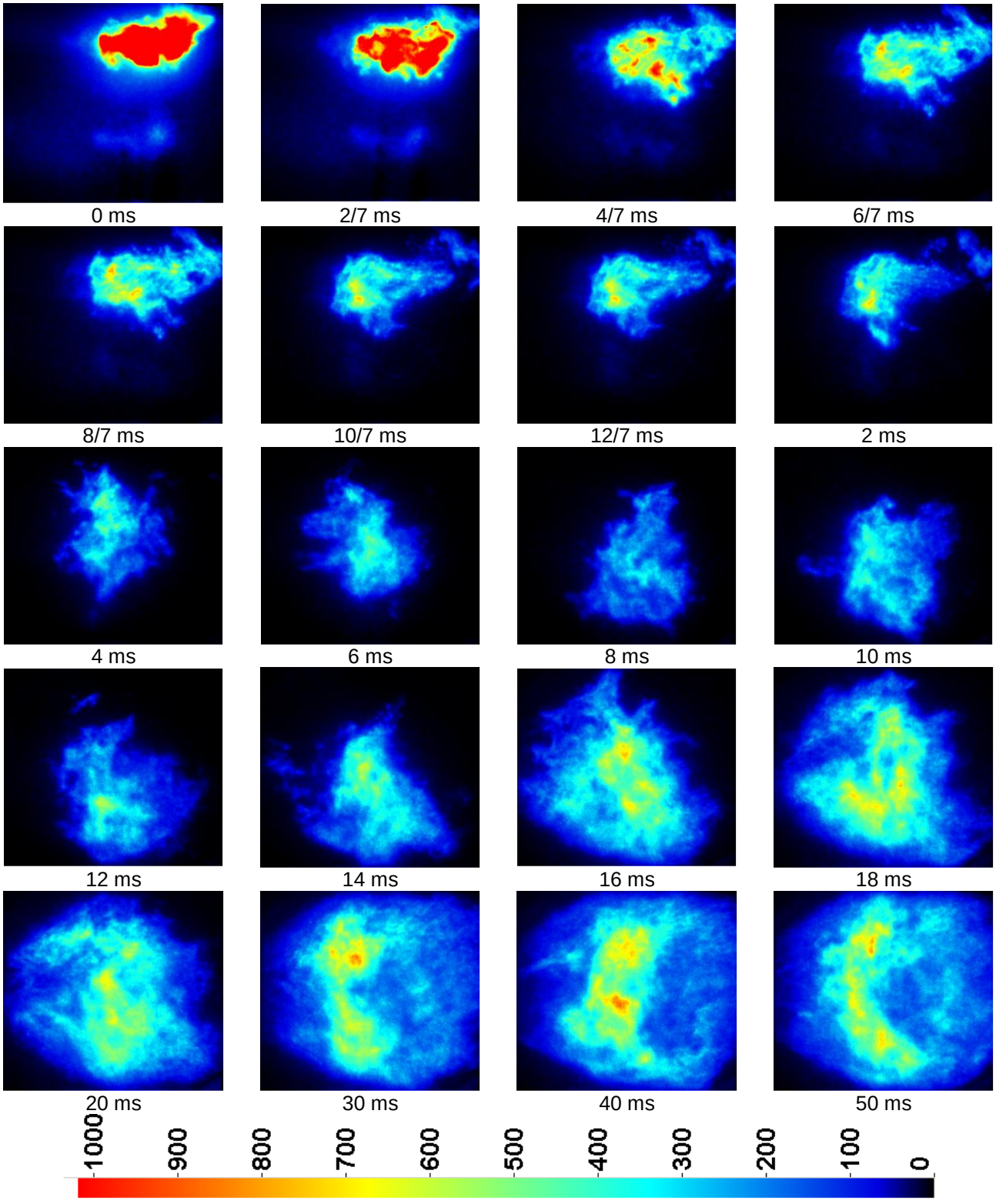

Figure A1. Temporal development of the UV emissions. Images were selected from a high-speed sequence comprising 1000 images. (Note that the time steps between the displayed images are not equal.)

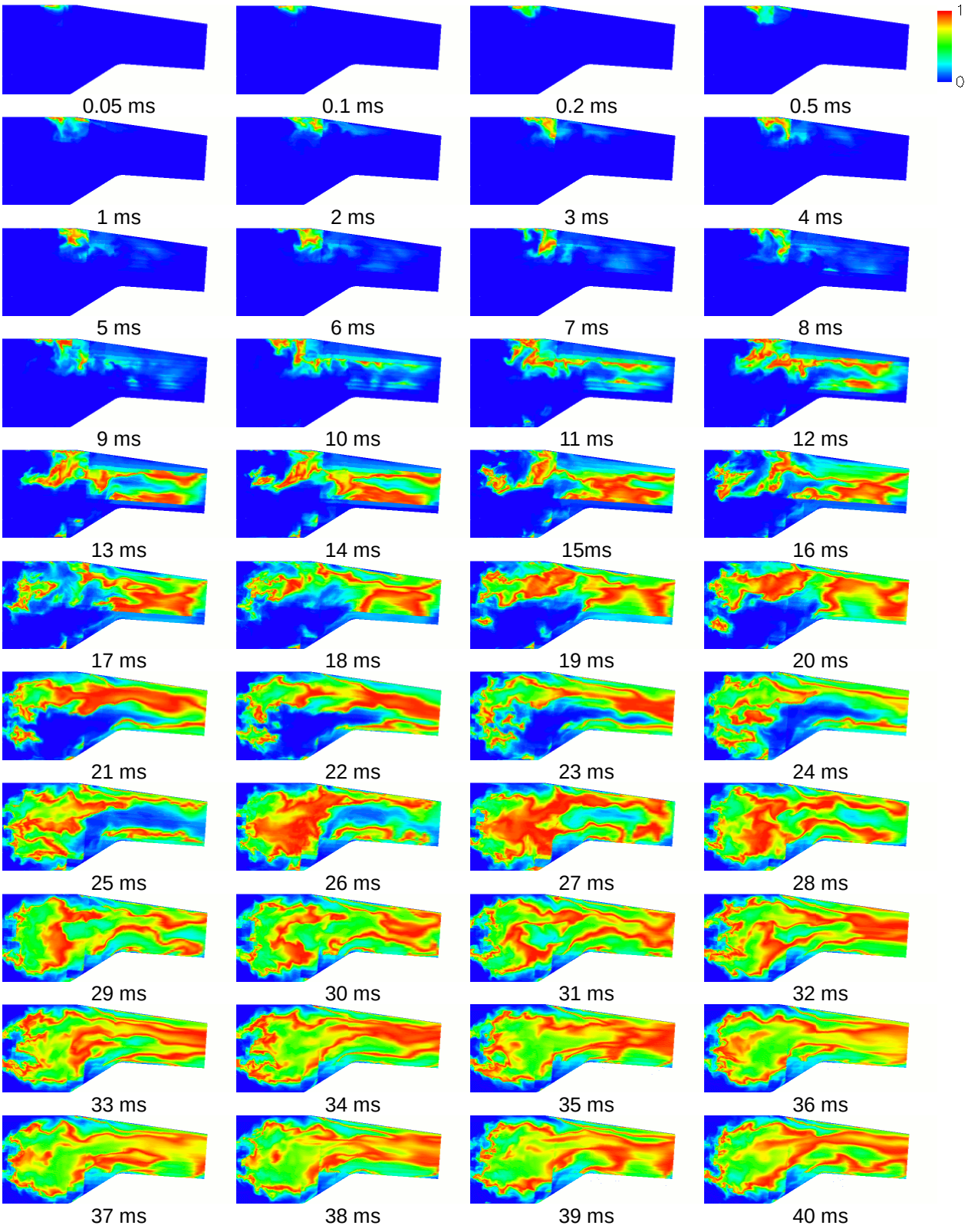

Figure A2. Time series of instantaneous normalized temperature in injector centreline plane for ignition simulation as predicted by CMC LES.